Received: 5 November 2023 | Revised: 5 February 2024 | Accepted: 8 March 2024 | Published online: 19 March 2024

RESEARCH ARTICLE

Archives of Advanced Engineering Science
2025, Vol. 3(1) 35–43
DOI: 10.47852/bonviewAAES42022009

BON VIEW PUBLISHING

A Digital Twin Development Framework for an Electrical Submersible Pump (ESP)

Mihiran Galagedarage Don[1], Sampath Liyanarachchi[1] and Thumeera R. Wanasinghe[2,*]

[1]*Department of Mechanical and Mechatronics Engineering, Memorial University of Newfoundland, Canada*

[2]*Department of Electrical and Computer Engineering, Memorial University of Newfoundland, Canada*

Abstract: Premature failure of a subsystem can be critical for an industrial cyber-physical system (CPS). A digital twin (DT)-assisted predictive maintenance procedure can reduce the risk of costly unplanned maintenance. This study presents a generalized DT development framework for an electrical submersible pump (ESP) that can assist in predictive maintenance. The framework is applied on a single-phase ESP as a proof of concept. The maximum winding temperature of the selected ESP is simulated using a multiphysics simulation tool with transient electromagnetic and transient heat transfer solvers. The simulation parameters were refined using data captured through an ESP free-run experiment. Simulating the total energy loss in the ESP stator and rotor and the transfer of heat from the outer fluid domain facilitates a relationship between the measurable external temperature and the maximum temperature in the stator winding. Following a design of experiment approach, a series of simulations were run to establish a statistical model for the winding temperature in terms of the fluid temperature, the time duration a particular temperature was persistent, and the initial maximum stator winding temperature. As the instantaneous maximum stator winding temperature is related to the remaining useful lifetime, it was shown using a case study that the proposed framework can prognosticate the ESP failure, assisting effective decision-making for predictive maintenance of a CPS.

Keywords: cyber-physical systems, digital twin, electrical submersible pump, predictive maintenance

1. Introduction

To maintain a competitive edge in the industrial landscape, predictive maintenance of cyber-physical systems (CPS) plays a major role in ensuring continuous operations and enhancing the productivity of industrial systems. Reliable operation of subsystems, such as electrical submersible pumps (ESP) used in the oil and gas, geothermal, wastewater, mining, agriculture, and construction industries, is essential to avoid catastrophic failure and unplanned shutdowns while reducing risks. Among these applications, ESP is one of the most popular artificial lift-pumping devices used in more than 60% of the world's oil production. They are employed in more than 90% of offshore oil wells for lifting oil and other hydrocarbons to the surface [1]. Nevertheless, the failure probability appears to be high, causing millions of oil barrel losses, leading to a high production risk. Similar challenges are experienced in the geothermal energy generation sector where ESPs are being used for lifting geothermal fluids [2, 3] that could reach 150–300 °C [4]. With reference to the monitoring and maintenance of ESPs, it is highly expensive as substantial expert interactions via frequent well visits are necessary [5]. This brings up the need for a failure prognosis and predictive maintenance approach that can avoid ESP failures in oil production wells.

Recently, digital twin (DT)-enabled systems have emerged as reliable and cost-effective for fault detection and diagnosis [6–10]. In this study, we propose to deploy DT for ESP fault detection and remaining useful life (RLT) calculation. The proposed DT focuses on ESP stator winding failure prognosis and DT-based RLT prediction. This DT framework was implemented on a practical ESP (i.e., VEVOR 45DM3/6 ESP), and outcomes were compared with experimental results. This approach can be effectively utilized in predictive maintenance-related decision-making.

In this article, Section 2 introduces DTs and their potential use in the predictive maintenance of CPSs. Section 3 provides a detailed description of the development of a DT which predicts the stator winding lifetime of an induction motor. A case study is also presented to demonstrate the use of the developed methodology. A discussion is provided in Section 4 followed by the conclusion in Section 5 and further work in Section 6.

2. Background

2.1. Potential uses of DTs in predictive maintenance over the currently available techniques

The conventional methods in ESP maintenance involve technicians being physically present at the well site to take measurements, followed by expert judgments. This approach was then developed for remote measurements and computer-aided

*Corresponding author: Thumeera R. Wanasinghe, Department of Electrical and Computer Engineering, Memorial University of Newfoundland, Canada. Email: thumeerawa@mun.ca

analysis [11]. As described in Peng et al. [1], although ammeter charts have been used as ESP failure diagnostic tool for a long time, it has some inherent operational and performance limitations. This technique monitors the motor current and logs it on a circular chart as a function of time. Although the method can be employed to detect a complete ESP failure, it is less suitable to identify and isolate component-level failures.

According to Awaid et al. [12], physical quantities of ESPs, such as discharge pressures, intake and motor temperatures, vibration, and current leakage, are continuously monitored by real-time down-hole sensors in most production wells. Although the raw data are often misleading, the relevant technologies are available to interpret the required data to identify cases such as holes in tubing, shut-in at the surface, ESP wear, blockage at pump intake, debris in the pump, broken shaft, change in reservoir pressure, and blockage at perforations. This has been mainly done using pattern recognition approaches [12]. Furthermore, several machine learning (ML) and statistical approaches in the literature facilitate performance optimization and anomaly detection, such as support vector classifiers, random forest classifiers, and principal component analysis [1]. However, the continuous monitoring of the ESP's lifetime decay is not presented.

The DT technology can be used to replicate electromagnetic [13], electrical, and thermal [14, 15] devices for status monitoring purposes. Therefore, as a step forward, a DT of an ESP can be developed to analyze the performance, which provides a broader range of flexibility. For example, a series of "what-if" scenarios can be run with DTs to explore potential failures that have never been experienced. The relevant data patterns can be used for training ML algorithms for failure classifications. The knowledge gathered through the DT will help to detect failure modes, including the modes yet to occur, and hence, the project risks can be reduced by implementing proper predictive maintenance practices. It will also be a solution for the uncooperative data-sharing policies and practices in the oil and gas field due to the consistently growing competition among the oil and gas operators and supply chain companies. Moreover, the DT will make a considerable contribution to the research and development sector of the oil and gas field due to the aforementioned reasons.

Although there have been many works on DT, there is still no accepted definition, unified framework, or method of implementation [15]. As defined in DAU [16], a DT can be introduced as an "integrated multi-physics, multi-scale, probabilistic simulation of an as-built system, enabled by digital thread, that uses the best available models, sensor information, and input data to mirror and predict activities/performance over the life of its corresponding physical twin." Meanwhile, Dymond et al. [17] concludes that this is the broadest definition available in the literature. It has a wide application range, including cyberattack detection [18] and automation [19].

2.2. Probable causes of ESP's anomalous behaviors and their effect on its useful lifetime

ESPs are employed in offshore and onshore wells at various depths and under diverse wellbore and fluid conditions. The reliability of the ESP's function has a more significant impact on the operation cost and personal safety. An ESP can deviate from its normal operating condition for numerous reasons, including electrical, mechanical, and structural failures.

The study presented in this article focuses on ESP stator insulation failure due to high temperatures. According to Chelmiah and Kavanagh [20], the breakdown of machinery is attributed to insulation failure of induction motors, accounting for as much as 66% of such incidents. It represents a particularly difficult domain for the formulation of condition-based monitoring techniques. As mentioned in Gokdere et al. [21], the winding temperature affects the life expectancy of motor winding insulation, and the degree of damage depends on the insulation material class. For every 10 °C increase in temperature, the average life expectancy of class *H* insulation is approximately reduced by 50%. Figure 1 [17] depicts a typical insulation life expectancy against the temperature curve, while Equation (1) is the mathematical model

Figure 1
Typical winding insulation life versus temperature curve

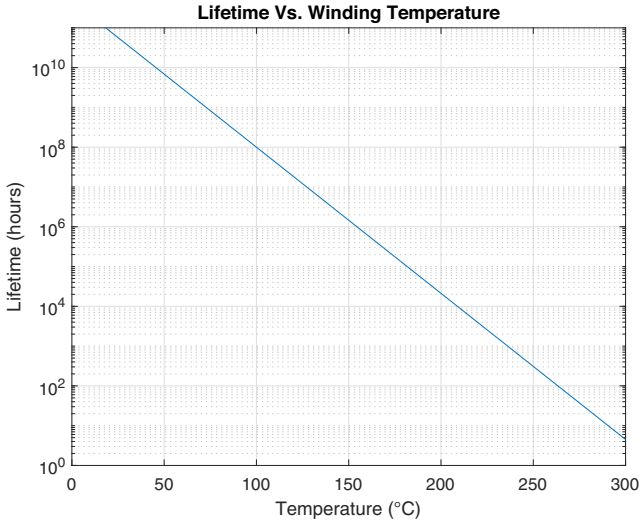

$$\log(PL) = -\frac{5.8}{150} T_{max} + \frac{178}{15} \quad (1)$$

As further discussed in Dymond et al. [17], failures of the ground wall or the turn insulation are typically caused by stator winding failures. The corresponding failure mechanism is referred to as the slow emergence of an insulating deficit. This weakness is typically brought on by a trapped vacuum that keeps growing as a result of persistent corona or partial discharge activity. In addition to inside-out failure mode, recent research on actual machine failures and studies of coils on voltage endurance tests suggest that breakdowns might start from the outside surface as well. Contamination of the surface causes significant surface discharge and tracking. The quick winding failure that might result from this surface discharge is caused by the corona activity's inward migration.

Direct measurement of winding temperature is practically difficult when the ESP is in operation. Therefore, an indirect measurement technique is required to estimate the internal temperature of the winding. A DT can be used to simulate winding heat generation and subsequent transfer to the fluid flow through the pump housing. The heat flows into the pump at higher fluid temperatures, which can also be simulated. In other words, a DT can be employed to run a series of "what-if" scenarios and a series of simulations in developing statistical models following the design of experiment (DOE) approach. In this way, a knowledge base can be developed in the form of statistical models and simulated data, which can be used in real-time estimations. The following section

provides a detailed explanation of the development of a DT for a given ESP and the way to determine the RLT.

3. Methodology and Results

This section explains the approach of DT development of a commercially available ESP. The methodology can be adapted to develop DTs of different types of ESPs and induction motors. The process starts with the determination of ESP's parameters by dismantling and sectioning. Based on the measurements, the electromagnetic simulation was done to determine the core and winding losses of the stator and rotor. Based on the loss estimations, the heat transfer model was developed, which was refined to improve the accuracy with the help of an experimental result. The refined model was then used to develop a statistical model using a DOE approach. The statistical model and the decay model presented in Equation (1) were employed to determine the instantaneous RLT of the stator winding. The proposed framework was applied in a case study as a proof of concept. The process is depicted in Figure 2. In this diagram, T_{max} stands for the maximum winding temperature, while T_{max0} represents the initial maximum temperature. The ESP's surface temperature and its persistent time are designated as T_s and t_p, respectively. The relationships among the variables are further explained in Section 3.

Figure 2
Methodology overview

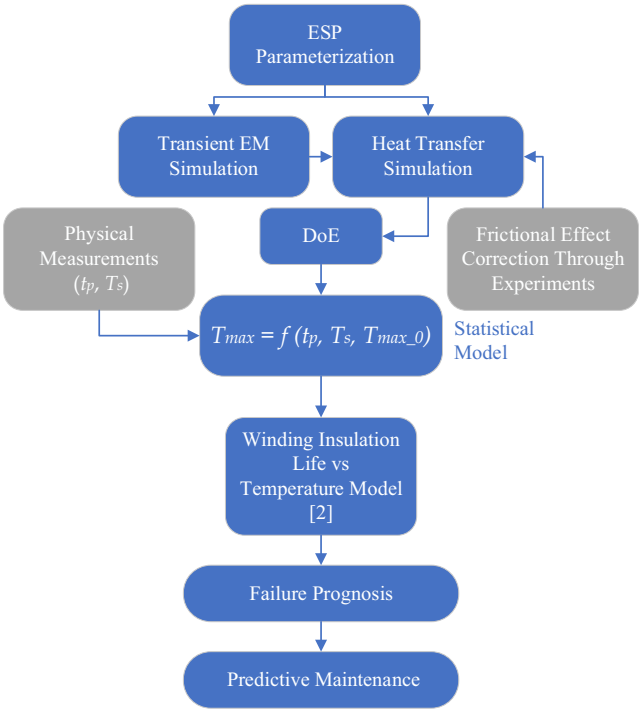

3.1. Parameters and determination of the ESP

A commercially available single-phase ESP (VEVOR 45DM3/6) was selected, shown in Figure 3, and the induction motor parameters were determined by manual measurements of the stator and rotor after dismantling and sectioning. Figure 4(a) and 4(b) depicts the construction of the stator, which is a distributed winding with a Slot-AC type core. The rotor shown in Figure 5(a) and 5(b) consists of a squirrel cage-type core. A detailed parameter list is presented in Table 1.

Figure 3
VEVOR 45DM3/6 ESP

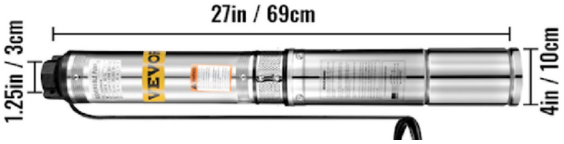

Figure 4
Stator of the selected ESP. (a) Sectioned stator coil. (b) Core and winding of the stator

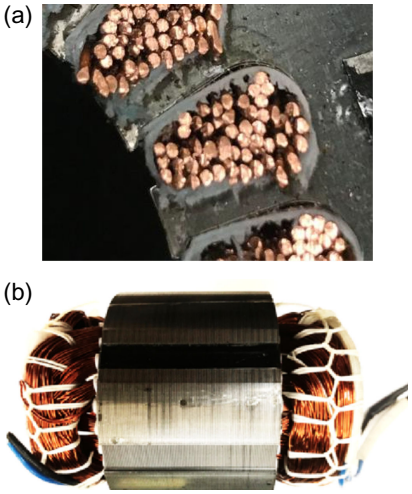

Figure 5
Rotor of the selected ESP. (a) Rotor of the selected ESP. (b) Sectioned rotor

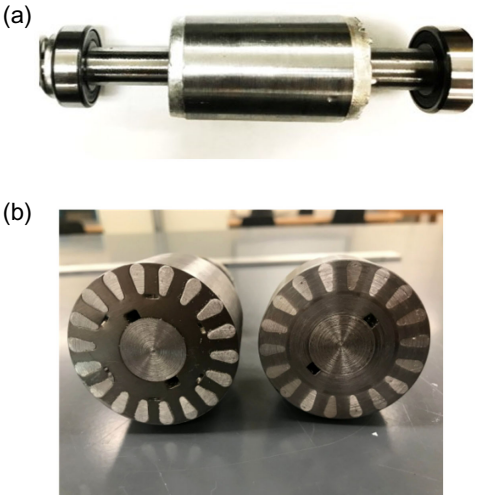

Table 1
Maxwell simulation parameters

Description	Value/material/design	Unit
Operation type	Motor	–
Load type	Constant speed	–
Rated output power	0.37	kW
Rated voltage	110	V
Rate speed	2850	rpm
Operating temperature	10	°C
Generic rotating machine		
Rated power factor	0.8	–
Capacitive power	No	–
Source type	AC	–
Structure	Inner rotor	–
Stator type	SLOT AC	–
Rotor type	SLOT CAGE	–
Stator		
Number of poles	4	–
Number of slots	24	–
Circuit type	C2	–
Slot type	1	–
Position control	No	–
Core		
Outer diameter	92	mm
Inner diameter	50	mm
Length	60	mm
Stacking factor	0.95	–
Steel type	Iron	–
Press board thickness	No press board	–
Magnetic press board	FALSE	–
Skew width	0	–
Lamination sectors	0	–
Slot		
Auto design	TRUE	
Hs0	0	mm
Bs0	0	mm
Winding layers	1	–
Winding type	Whole coiled	–
Parallel branches	1	–
Conductor per slot	50	–
Number of strands	1	–
Wire wrap	0.75	mm
Wire size	0.75	mm
Conductor type	Iron	–
Rotor		
Number of slots	18	–
Core		
Outer diameter	49	mm
Inner diameter	19	mm
Length	70	mm
Stacking factor	0.95	–
Steel type	Iron	–
Sleeve type	Conductor	–
Press board	6	mm
Shaft		
Magnetic shaft	FALSE	–
Friction loss	0	W
Windage loss or power	0	W
Reference speed	0	rpm

3.2. The electromagnetic simulation

The motor was simulated using ANSYS™ Electronics Desktop software based on the specifications determined through measurements and product specifications. RMxprt module in ANSYS™ Electronics Desktop was used for calculating winding and core losses of both stator and rotor. It is specialized in the design and analysis of rotating electrical machines and offers a simplified and template-based approach. The simulation inputs are presented in Table 1. The estimated loss calculations were transferred to the heat transfer simulation for further analysis.

3.3. The heat transfer simulation

ANSYS™ Transient Thermal was used to model the heat transfer through the shaft, rotor core, rotor "winding," stator core, and stator winding toward the housing of the ESP. Initially, the entire induction motor was modeled in SolidWorks™. Considering the symmetry, a portion of three stator winding slots and two rotor "winding" slots were selected for further analysis in ANSYS™ Transient Thermal. The shaft, rotor core, stator core, and housing were assigned material properties similar to that of steel, while the stator and rotor windings were assigned copper and aluminum, respectively. The insulation layer material around the stator winding was considered polyester. The thin air layer in between the stator and the rotor was defined as a new material with a conductivity of 10 times that of air. This is due to the severe shearing action that takes place within the air gap.

3.3.1. Modeling approach

There are several simplifying assumptions made to improve the efficiency of the transient thermal simulation. The fluid flow outside the ESP is considered to maintain a uniform temperature due to the mixing effect of the turbulent flow. This fluid flow sweeps the surface of the induction motor, enters the ESP impeller system, and flows upward. Further, for the heat transfer simulation, the 50 copper wires in a given stator slot are considered a monolithic copper bar due to their high thermal conductivity. The heat transfer was considered purely radial as there is no temperature gradient laterally. The heat generations estimated in the electromagnetic simulation were modeled as volume heat sources of windings and cores of both stator and rotor.

Moreover, the heat generation due to frictional effects is introduced as volumetric heat sources in the air gap between the stator and the rotor and edge of the shaft where the bearings are connected. The surface of the ESP housing was assumed to be a heat sink while maintaining a temperature over a specific time range. The heat transfer due to radiation and convection inside the pump was considered negligible compared to that of conduction.

Figure 6(a) illustrates the 3D model developed based on the parameters measured using the actual pump, and Figure 6(b) represents the portion of the full model used for the heat transfer simulation.

In Figure 6(b), the radial surfaces are set as adiabatic to ensure the radial heat transfer inside the volume considered. This transient heat transfer simulation can estimate the stator winding temperature with reference to the surface temperature of the housing controlled by the fluid being conveyed, facilitating the development of a statistical model to determine the real-time winding temperature based on the

Figure 6
The motor model and heat transfer simulation. (a) 3D model of the induction motor section of the ESP. (b) The considered section

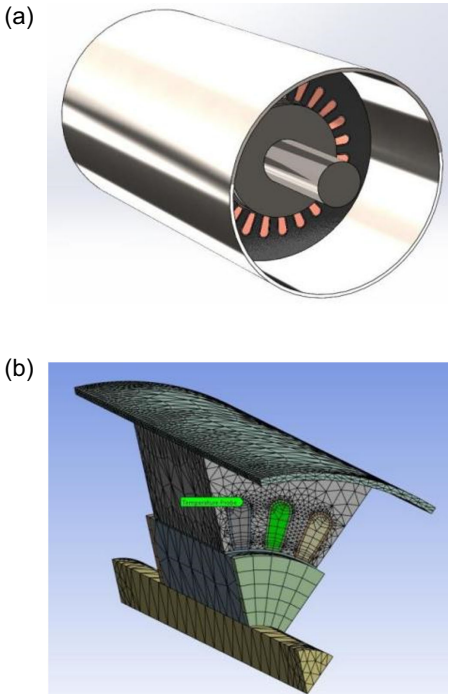

time (t_p) that a particular temperature has been persistent, the temperature (T_s) of the fluid flow, and the initial stator winding maximum temperature (T_{max0}).

3.4. Simulation refinement using experimental findings

Although the heat generation due to frictional effects is considerably high, there are practical challenges in determining the frictional coefficients effectively. As a solution, a simulation refinement using experimental results is proposed, which is discussed below.

The VEVOR 45DM3/6 pump was "free run," and the surface temperature change was captured experimentally. The pump was kept vertically, and a thermocouple was attached to its housing surface as illustrated in Figure 7. The readings were taken at 1 min intervals, while the pump was free running from room temperature. The observed temperature variation is presented in Figure 8(a). The heat transfer simulation model introduced in Section 3 was reused with modifications. The housing surface was assigned a convection heat transfer coefficient ($h = 8$ W m^{-2}), calculated considering the pump as a vertical cylinder. The temperature variation indicated by the refined simulation model is presented in Figure 8(b). Compared with the experimental results presented in Figure 8(a), the refined model behaves with reasonable accuracy. This accuracy was achieved by fine-tuning the frictional heat generation source to match the experimental results. This approach incorporated the effect of friction into the simulation model.

Figure 7
ESP free-run experimental setup

Figure 8
Experimental results versus refined simulation model result. (a) Experiment results. (b) Behavior of the refined simulation model results

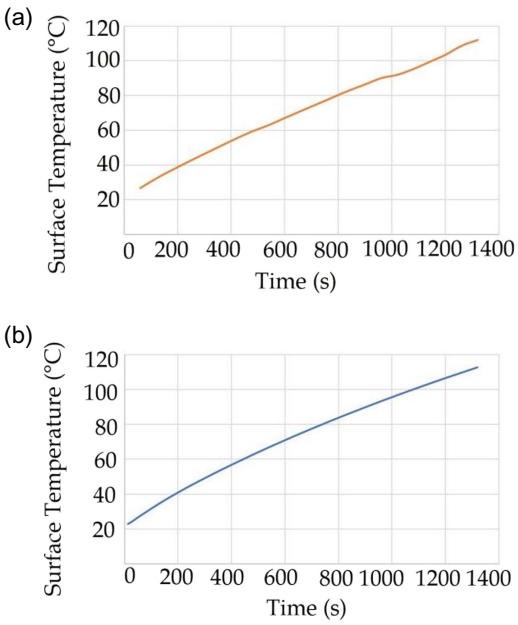

3.5. Development of the statistical model

The statistical models were developed following a DOE approach. The response surface method was employed while keeping *Ts*, T_{max0}, and t_p as the factors (i.e., independent variables) and the maximum stator winding temperature (T_{max}) as the response variable. The relationship is presented by Equation (2):

$$T_{\max} = f\left(t_p, T_S, T_{max0}\right) \tag{2}$$

Table 2
Factors and their ranges

Parameter	Range	Unit
Pump surface temperature	150–300	°C
Previous maximum temperature	150–300	°C
Duration of consistent temperature	1–600	s

Table 3
The experimental matrix for heat transfer model development

Experiment	Surface temp. (T_s)	Initial temp. (T_{max0})	Time duration (t_p)	Maximum stator winding temp. (T_{max})
1	300	225	300.5	304
2	225	300	300.5	233.8
3	225	225	300.5	232.7
4	225	225	300.5	232.7
5	225	225	300.5	232.7
6	300	150	1	150.9
7	150	150	1	150.8
8	225	150	300.5	231.5
9	150	150	600	160.0
10	225	225	300.5	232.7
11	225	225	600	231.8
12	150	300	600	160.3
13	150	300	1	300.8
14	225	225	300	232.7
15	225	225	300.5	232.7
16	300	300	600	303.8
17	300	300	1	300.8
18	225	225	1	225.8
19	300	150	600	303.4
20	150	225	300.5	161.6

The factors' ranges are presented in Table 2. The experimental matrix presented in Table 3 was followed to perform the experiments using the refined simulation model. The experiments were designed using Design Expert™ software.

The statistical model developed following the above methodology is presented in Equation (3). The model is also depicted in Figure 9(a) and 9(b). Figure 9(b) is the contour diagram of Figure 9(a). As illustrated, the maximum winding temperature becomes maximum when both the surface temperature and its persistent time are at their higher extremes. Conversely, the maximum winding temperature becomes minimum when the surface temperature is maintained consistently low for a prolonged time as expected.

$$(T_{\max}+1)^{0.5} = 15.13 + 1.42T_S + 1.02T_{max0} + 0.1094t_p + 1.19T_s t_p - 1.26T_{max0}t_p \quad (3)$$

Using Equation (3), the temperature of the stator winding can be estimated along with the time duration that a particular temperature persists. Using the lifetime decay model illustrated in Figure 1 [17], the RLT can be determined.

Figure 9
The statistical model for T_{max}. (a) 3D surface view of the model. (b) 2D contour view of the model

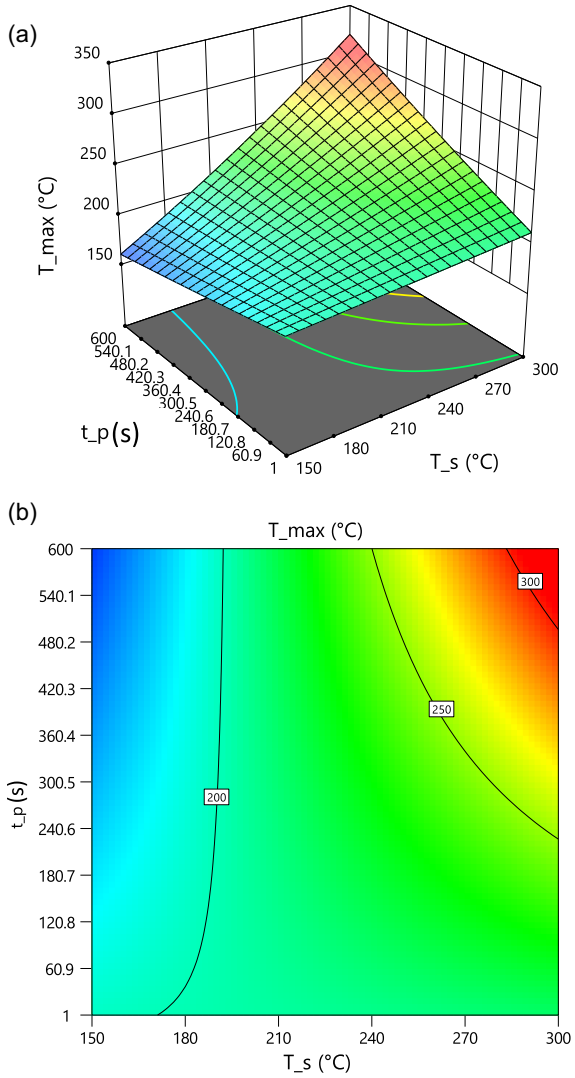

3.6. Case study

A random temperature fluctuation in the fluid flow pumped by the ESP throughout 3.5 days is considered, which is illustrated in Figure 10. The instantaneous RLT presented in Figure 11 was determined based on three factors: 1) the statistical model presented in Equation (3), 2) the winding insulation life decay model illustrated in Figure 1 [17], and 3) the temperature fluctuation presented in Figure 10.

The code developed to determine the lifetime decay follows the algorithm depicted in Figure 12. According to the algorithm, the calculation process starts from the practically feasible measurements (i.e., t_p and T_s). Using the developed statistical model presented in Equation (3), the T_{max} is calculated. The initial calculation cycle also requires the initial stator winding temperature (T_{max0}). For example, as illustrated in Figure 13, it can be taken as the steady-state temperature after the motor surface is subjected to a temperature of 225 °C for a duration of 300 s. This estimation of T_{max0} is the calibration of the system. The estimated T_{max} is then used in Equation (4) to determine the RLT:

Figure 10
Fluid flow temperature fluctuation with time

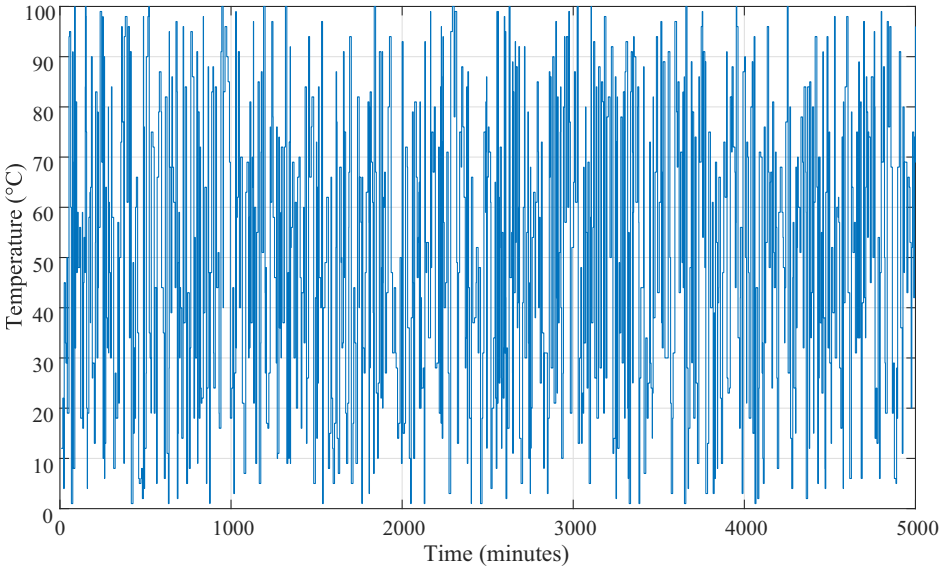

Figure 11
Instantaneous remaining useful life (RLT) versus time

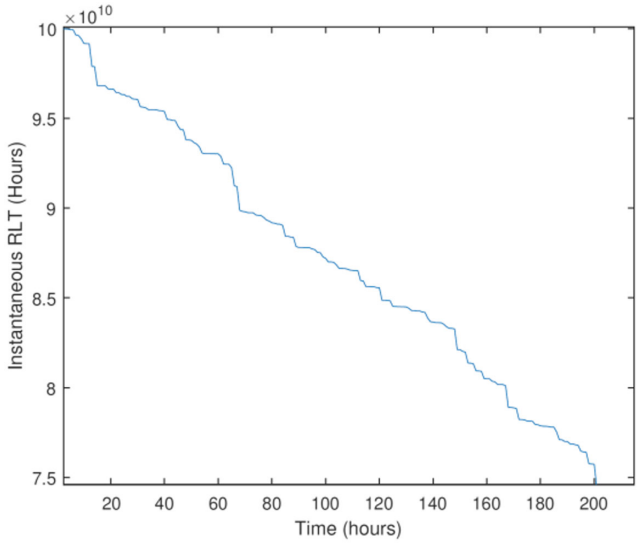

Figure 12
Algorithm of lifetime decay calculations

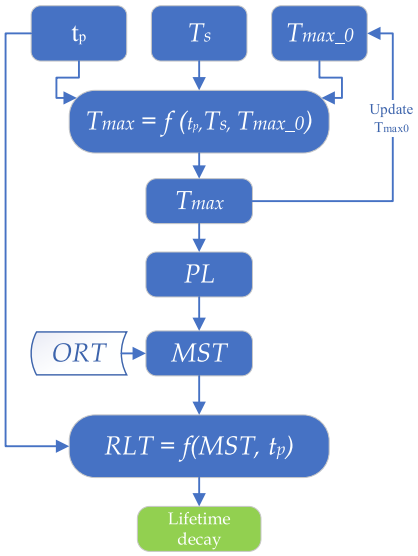

$$\mathrm{RLT} = f\left(MST,\ t_p\right) \tag{4}$$

where MST is a dimensionless number. RLT depicted in Figure 11 is a discrete function with a continually changing negative gradient. This negative gradient is defined with the dimensionless number named "MST's constant," which is presented in Equation (5).

$$\mathrm{MST} = \frac{ORL}{PL} \tag{5}$$

where ORL is the original reference lifetime and PL is the projected lifetime.

4. Discussion

As mentioned in Section 3, this study makes several simplifying assumptions to keep the simulations less complicated while keeping a required level of representation of the actual system. The simulation model section, illustrated in Figure 6(b), represents the entire induction motor considering the geometrical symmetry. Up on that, the heat transfer is purely radial as the temperature gradient is only in the radial direction, which supports the assumption. The heat generation is considered due to stator core loss, stator winding loss, rotor core loss, rotor winding loss, and frictional heat. The frictional heat component was corrected using the experimental results. The surface temperature (T_s) was considered uniform and equal to the instantaneous water flow temperature due to the turbulent and well-

Figure 13
The temperature change in stator winding for 225 °C surface temperature

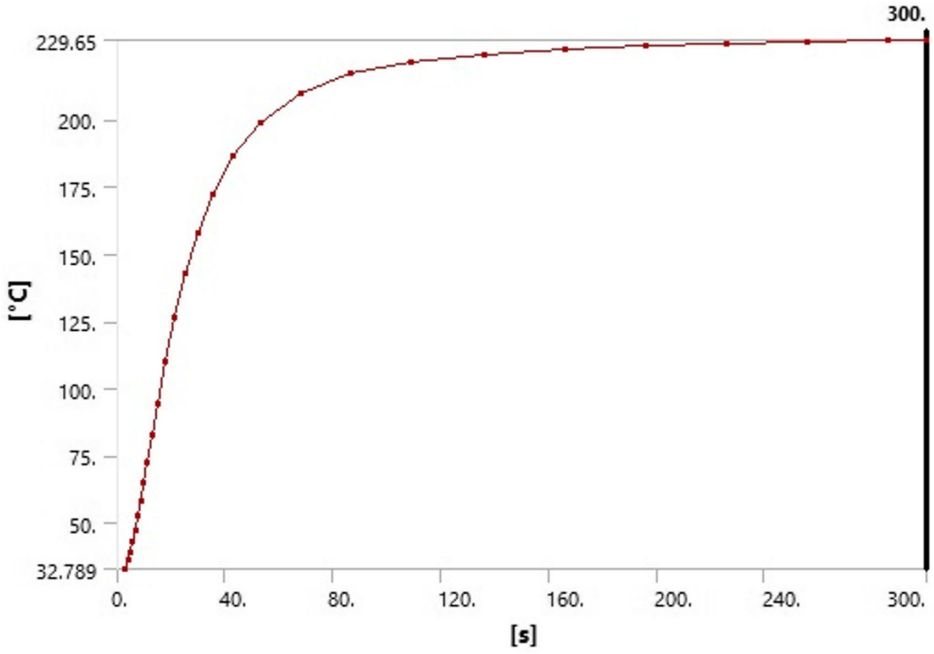

mixing nature of the flow. The 50 copper wires in the stator winding are modeled as a monolithic copper bar with a polyester insulation outer layer due to the high thermal conductivity of copper.

The thin air gap between the rotor and the stator was considered a conductive layer with almost 10 times the conductivity of air. This implies the main mode of heat transfer through the thin layer is due to conduction, while convection and radiation heat transfer through the thin air layer was considered negligible. The heat conducted to the rest of the motor cover and components is treated as negligible. The outer surface of the motor is mirror-finished; hence, the radiation heat transfer is minimized. Therefore, in the experimental validation, a convection heat transfer coefficient of 8 W m^{-2} was assigned through a calculation assuming a vertical cylindrical surface.

Furthermore, in assigning the materials for the heat transfer model, the lamella nature of the cores and the insulation layer between the lamella structure are not considered. Instead, both the cores are considered to be made out of iron in the monolithic form.

This study is limited to the lifetime prognosis of stator windings of an ESP induction motor section due to high-temperature effects. The lifetime is decided based on the degradation of the insulation layer. It is an accumulating failure analogous to fatigue failure in metals, where the rate depends on the instantaneous temperature only. The dimensionless number introduced (i.e., MST) makes the bridge between the decay model available in the literature (i.e., Figure 1 [17]) and the accumulation of decay (Figure 11).

5. Conclusion

This study presents a DT development framework for an ESP to determine the RLT of its stator winding. The scope is limited to the decay of the insulation layer due to elevated operating temperatures. The framework development process starts with the determination of the design parameters of the ESP, followed by an electromagnetic simulation and a heat transfer simulation. A statistical model that can estimate the internal stator winding temperature was developed following a DOE approach. A typical insulation layer decay model available in the literature was employed to estimate the instantaneous RLT, which is an important piece of information for predictive maintenance practices. The developed framework was applied to a case study as a proof of concept. In general, the framework can be adapted to develop DTs for real-time monitoring of the RLT of ESPs due to overheating. Hence, it can reduce the risk associated with processes employed with induction motors.

6. Further Work

The DT introduced through this study can be further expanded to prognose other types of failures. In this way, the DT will be able to predict the actual lifetime defined by all the potential failure mechanisms.

Funding Support

The authors thankfully acknowledge the financial support provided by Seed, Bridge and Multidisciplinary Fund of Memorial University of Newfoundland, Canada.

Conflicts of Interest

The authors declare that they have no conflicts of interest to this work.

Data Availability Statement

The information/data required for reproducing the results is already presented in the manuscript.

Author Contribution Statement

Mihiran Galagedarage Don: Conceptualization, Methodology, Software, Formal analysis, Data curation, Writing – original draft, Visualization, Project administration. **Sampath Liyanarachchi:** Investigation, Writing – review & editing. **Thumeera R. Wanasinghe:** Conceptualization, Methodology, Software, Validation, Resources, Writing – review & editing, Supervision, Project administration.

References

[1] Peng, L., Han, G., Sui, X., Pagou, A. L., Zhu, L., & Shu, J. (2021). Predictive approach to perform fault detection in electrical submersible pump systems. *ACS Omega*, *6*(12), 8104–8111. https://doi.org/10.1021/acsomega.0c05808

[2] National Renewable Energy Lab. (2014). *Electronic submersible pump (ESP) technology and limitations with respect to geothermal systems (fact sheet)*. Retrieved from: https://www.osti.gov/biblio/1159333

[3] Rahman, A., Farrok, O., & Haque, M. M. (2022). Environmental impact of renewable energy source based electrical power plants: Solar, wind, hydroelectric, biomass, geothermal, tidal, ocean, and osmotic. *Renewable and Sustainable Energy Reviews*, *161*, 112279. https://doi.org/10.1016/j.rser.2022.112279

[4] Stober, I., & Bucher, K. (2021). *Geothermal energy: From theoretical models to exploration and development*. Germany: Springer.

[5] Bates, R., Cosad, C., Fielder, L., Kosmala, A., Hudson, S., Romero, G., & Shanmugam, V. (2004). Taking the pulse of producing wells—ESP surveillance. *Oilfield Review*, *16*(2), 16–25.

[6] Feng, K., Xu, Y., Wang, Y., Li, S., Jiang, Q., Sun, B., . . . , & Ni, Q. (2023). Digital twin enabled domain adversarial graph networks for bearing fault diagnosis. *IEEE Transactions on Industrial Cyber-Physical Systems*, *1*, 113–122. https://doi.org/10.1109/TICPS.2023.3298879

[7] Hasan, M. N., Jan, S. U., & Koo, I. (2023). Wasserstein GAN-based digital twin inspired model for early drift fault detection in wireless sensor networks. *IEEE Sensors Journal, 23*(12), 13327–13339. https://doi.org/10.1109/JSEN.2023.3272908

[8] Li, T., Shi, H., Bai, X., & Zhang, K. (2023). A digital twin model of life-cycle rolling bearing with multiscale fault evolution combined with different scale local fault extension mechanism. *IEEE Transactions on Instrumentation and Measurement*, *72*, 1–11. https://doi.org/10.1109/TIM.2023.3243663

[9] Wu, X., Lian, W., Zhou, M., Song, H., & Dong, H. (2023). A digital twin-based fault diagnosis framework for bogies of high-speed trains. *IEEE Journal of Radio Frequency Identification*, *7*, 203–207. https://doi.org/10.1109/JRFID.2022.3216331

[10] Xu, Y., Sun, Y., Liu, X., & Zheng, Y. (2019). A digital-twin-assisted fault diagnosis using deep transfer learning. *IEEE Access*, *7*, 19990–19999. https://doi.org/10.1109/ACCESS.2018.2890566

[11] Shuwaikhat, H. A., Ramos, M., Aifan, A. R., & Al-Sadah, A. A. (2017). Innovative approach to prolong ESP run life using algorithmic models. In *Abu Dhabi International Petroleum Exhibition & Conference*. https://doi.org/10.2118/188807-MS

[12] Awaid, A., Al-Muqbali, H., Al-Bimani, A., Al-Yazeedi, Z., Al-Sukaity, H., Al-Harthy, K., & Baillie, A. (2014). ESP well surveillance using pattern recognition analysis, oil wells, petroleum development Oman. In *IPTC 2014: International Petroleum Technology Conference*. https://doi.org/10.3997/2214-4609-pdb.395.IPTC-17413-MS

[13] Zhang, B., Zhang, M., Dong, T., Lu, M., & Li, H. (2023). Design of digital twin system for DC contactor condition monitoring. *IEEE Transactions on Industry Applications*, *59*(4), 3904–3909. https://doi.org/10.1109/TIA.2023.3256978

[14] Boglietti, A., Cavagnino, A., Lazzari, M., & Pastorelli, A. (2002). A simplified thermal model for variable speed self cooled industrial induction motor. In *Conference Record of the 2002 IEEE Industry Applications Conference. 37th IAS Annual Meeting*, *2*, 723–730. https://doi.org/10.1109/IAS.2002.1042640

[15] Hung, M. H., Lin, Y. C., Hsiao, H. C., Chen, C. C., Lai, K. C., Hsieh, Y. M., . . . , & Cheng, F. T. (2022). A novel implementation framework of digital twins for intelligent manufacturing based on container technology and cloud manufacturing services. *IEEE Transactions on Automation Science and Engineering*, *19*(3), 1614–1630. https://doi.org/10.1109/TASE.2022.3143832

[16] DAU. (2022). *Digital prototype*. [Online]. Retrieved from: https://www.dau.edu/glossary/digital-prototype

[17] Dymond, J. H., Stranges, N., Younsi, K., & Hayward, J. E. (2002). Stator winding failures: Contamination, surface discharge, tracking. *IEEE Transactions on Industry Applications*, *38*(2), 577–583. https://doi.org/10.1109/28.993182

[18] Balta, E. C., Pease, M., Moyne, J., Barton, K., & Tilbury, D. M. (2024). Digital twin-based cyber-attack detection framework for cyber-physical manufacturing systems. *IEEE Transactions on Automation Science and Engineering*, *21*(2), 1695–1712. https://doi.org/10.1109/TASE.2023.3243147

[19] Wang, T., Cheng, J., Yang, Y., Esposito, C., Snoussi, H., & Tao, F. (2022). Adaptive optimization method in digital twin conveyor systems via range-inspection control. *IEEE Transactions on Automation Science and Engineering*, *19*(2), 1296–1304. https://doi.org/10.1109/TASE.2020.3043393

[20] Chelmiah, E. T., & Kavanagh, D. F. (2022). Acoustic sensor array topologies for partial discharge localisation in electric machines. In *2022 International Conference on Electrical Machines*, 1582–1588. https://doi.org/10.1109/ICEM51905.2022.9910954

[21] Gokdere, L. U., Chiu, S. L., Keller, K. J., & Vian, J. (2005). Lifetime control of electromechanical actuators. In *2005 IEEE Aerospace Conference*, 3523–3531. https://doi.org/10.1109/AERO.2005.1559655

How to Cite: Don, M. G., Liyanarachchi, S., & Wanasinghe, T. R. (2025). A Digital Twin Development Framework for an Electrical Submersible Pump (ESP). *Archives of Advanced Engineering Science*, *3*(1), 35–43. https://doi.org/10.47852/bonviewAAES42022009